iScience

CellPress
OPEN ACCESS

Article

The role of mitochondrial autophagy in osteoarthritis

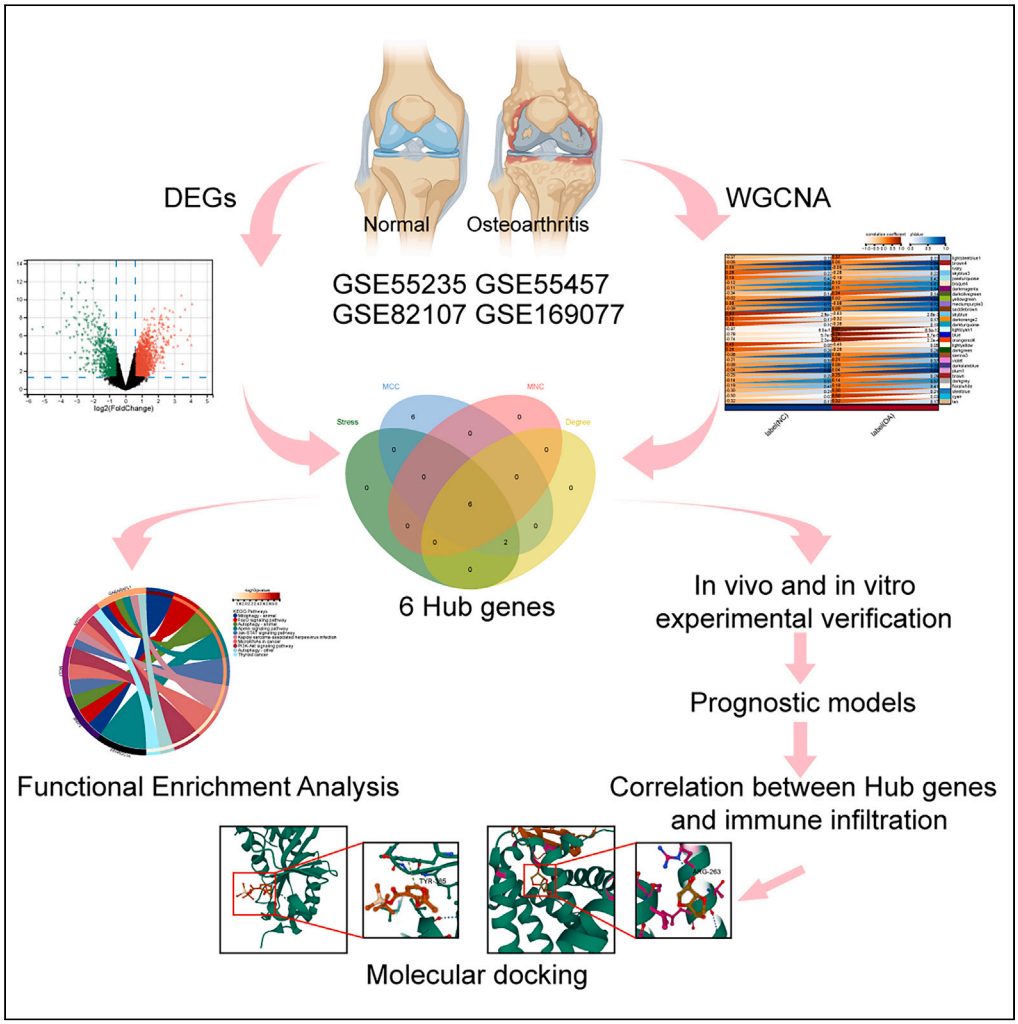

Genchun Wang, Xiong Zhang, Jingting Xu, Liangcai Hou, Zhou Guo, Kai Sun, Fengjing Guo

1085844308@qq.com (K.S.)
guofjdoc@163.com (F.G.)

Highlights

Analyzed mechanisms of mitochondrial autophagy-related genes and osteoarthritis

GSEA, WGCNA, GO, and KEGG analysis revealed biological processes

BNIP3 potential therapeutic target for osteoarthritis

Developing hub gene diagnostic model and immune correlation

Wang et al., iScience 27, 110741
September 20, 2024
https://doi.org/10.1016/j.isci.2024.110741

iScience

CellPress
OPEN ACCESS

Article

The role of mitochondrial autophagy in osteoarthritis

Genchun Wang,[1,2,3] Xiong Zhang,[1,3] Jingting Xu,[1] Liangcai Hou,[1] Zhou Guo,[1] Kai Sun,[1,*] and Fengjing Guo[1,4,*]

SUMMARY

Osteoarthritis (OA) is a progressive degenerative joint disease, and the underlying molecular mechanisms of OA remain poorly understood. This study aimed to elucidate the relationship between mitochondrial autophagy and OA by identifying key regulatory genes and their biological functions. Utilizing bioinformatics analyses of RNA expression profiles from the GSE55235 dataset, we identified 2,136 differentially expressed genes, leading to the discovery of hub genes associated with mitochondrial autophagy and OA. Gene set enrichment analysis (GSEA) revealed their involvement in critical pathways, highlighting their potential roles in OA pathogenesis. Furthermore, our study explored the immunological landscape of OA, identifying distinct immune cell infiltration patterns that contribute to the disease's inflammatory profile. We also evaluated the therapeutic potential of drugs targeting these hub genes, suggesting potential approaches for OA treatment. Collectively, this study advances our knowledge of mitochondrial autophagy in OA and proposes promising biomarkers and therapeutic targets.

INTRODUCTION

Osteoarthritis (OA), the most common degenerative joint disease globally, substantially impacts life quality with symptoms such as joint deformity and functional loss.[1–4] Pathologically, OA is characterized by articular cartilage destruction, synovial hyperplasia, osteophytes, and subchondral bone sclerosis, yet its pathogenesis and molecular intricacies remain elusive.[5] Current OA management primarily revolves around pharmacological interventions and surgery.[6]

Autophagy, a cellular homeostasis mechanism, plays a dual regulatory role in the progression of OA. It protects chondrocytes from oxidative stress in the early stages, while in the advanced stages, diminished autophagy contributes to cartilage degradation.[7,8] Mitophagy, a subtype of autophagy crucial for chondrocyte mitochondrial health, involves key molecules such as PINK1, PRKN, BNIP3, and MFN2. The PINK1-PRKN pathway, particularly studied in nucleus pulposus cells (NP cells) and chondrocytes, offers promising therapeutic insights for OA,[9] though its detailed regulatory mechanisms in OA require further exploration.

The advent of bioinformatics has greatly advanced protein research, aiding in the elucidation of protein functions, molecular pathways, and drug development.[10] This approach has been pivotal in uncovering OA pathogenesis and identifying potential therapeutic targets. Key differentially expressed genes (DEGs) and biomarkers such as circRNAs and ferroptosis-related genes have been identified in OA through bioinformatics analyses,[11–13] contributing to a growing repository of potential disease markers and potential therapeutic avenues.[14–16]

However, challenges like sample heterogeneity and confounding factors limit the accuracy of differential biomarkers. To mitigate these issues, a combination of DEGs, weighted co-expression networks (WGCNA), and validation across multiple independent datasets is recommended for comprehensive analyses. Our study utilizes microarrays and bioinformatics to construct a gene regulatory network around mitochondrial autophagy in OA.

RESULTS

The identification of hub genes that regulate mitochondrial autophagy and OA

To investigate the relationship between mitophagy and osteoarthritis (OA), we conducted a comprehensive analysis (Figure 1). First, we identified 2,136 DEGs from GSE55235 using the screening conditions "$p < 0.05$ and |logFC|>1.5" (Table S1). A volcano plot shows these DEGs (Figure 2A). Heat maps for the top 20 DEGs were plotted (Figure 2B). We constructed a weighted gene co-expression network from GSE55235 after removing aberrant samples and filtering genes. Using a soft threshold force of 5, the scalar independence reached 0.87

[1]Department of Orthopedics, Tongji Hospital, Tongji Medical College, Huazhong University of Science and Technology, Wuhan, Hubei 430030, China
[2]Orthopedic Medical Center, Union Hospital, Fujian Medical University, Fuzhou, Fujian 350000, China
[3]These authors contributed equally
[4]Lead contact
*Correspondence: 1085844308@qq.com (K.S.), guofjdoc@163.com (F.G.)
https://doi.org/10.1016/j.isci.2024.110741

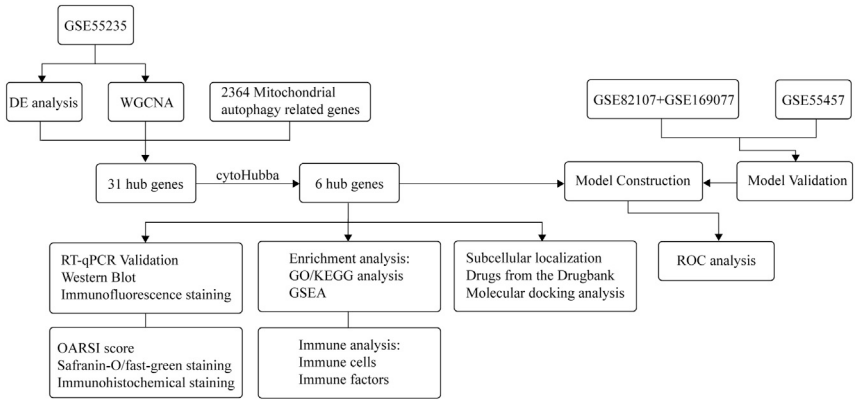

Figure 1. Flowchart of the study

and the average connectivity reached 69.86 (Figure 3A). As a result of dynamic tree-cutting with a sensitivity set to 3, a minimum module size of 30, and a module merging threshold of 0.25, 31 different co-expression modules were identified (Table 1) (Figure 3B), along with module feature vector clustering (Figure 3C). A correlation analysis was subsequently conducted between each module and clinical traits. There was the highest positive correlation between the MElightcyan1 module and OA (r = 0.97), while there was the highest negative correlation between the MEskyblue module and OA (r = −0.63) (Figure 3D). Here, the MElightcyan1 module, which contains 1,594 genes, has the largest absolute correlation and is selected for additional analysis to enrich the MElightcyan1 module genes. A total of 269 genes with high connectivity in the clinically significant module were identified as hub genes based on the cut-off criteria (| Module Membership [MM] | > 0.8). The Pearson correlation analysis revealed significant associations between the identified hub genes and OA, with p values less than 0.05. This statistical robustness underscores the strength of these genes' correlations with OA pathogenesis. According to MM and Gene Signifificance (GS) correlation analysis, these genes may have a strong association with modules and phenotypes (COR = 0.98, $p < 0.01$) (Figure 3E). When the sensitivity is set to 3, the minimum module size is set to 30, and the module merging threshold is set to 0.25, 29 separate co-expression modules can be obtained by dynamic tree cutting, and a gene clustering dendrogram was drawn being dependent on the results (Figure 3F). In addition, we clustered the samples of the GSE55235 dataset to obtain a clustering dendrogram of the NC and OA groups (Figure 3G) Through the intersection of 2,136 differential genes (Tables S1 and S4), 269 MElightcyan1 module hub genes (Table S2), and 2,364 mitochondrial autophagy-related genes screened (Table S3) by GSE55235, 31 hub genes related to mitochondrial autophagy and OA was obtained (Figure 4A). The STRING database was used to construct a Protein-Protein Interaction Networks (PPI) network that was used to reveal the interactions of each protein. The PPI network was actuated by the degree of target connectivity (DEgree) from largest to smallest (Figure 4B). Four cytoHubba algorithms (degree, Maximum Neighborhood Component [MNC], stress, and Maximal Clique Centrality [MCC]) were consistently able to determine hub genes. The six genes with the highest score were thought hub genes for OA (Table 2), namely MYC, BNIP3, GABARAPL1, PPARGC1A, MCL1, and BAG3 (Figures 4C and 4D). The violin plot shows that in GSE55235, the expression levels of MYC, BNIP3, GABARAPL1, MCL1, and BAG3 are significantly decreased in the OA group compared to the normal group ($p < 0.05$) (Figure 5A). Confirming the relevance of these observed results highlights their potential roles

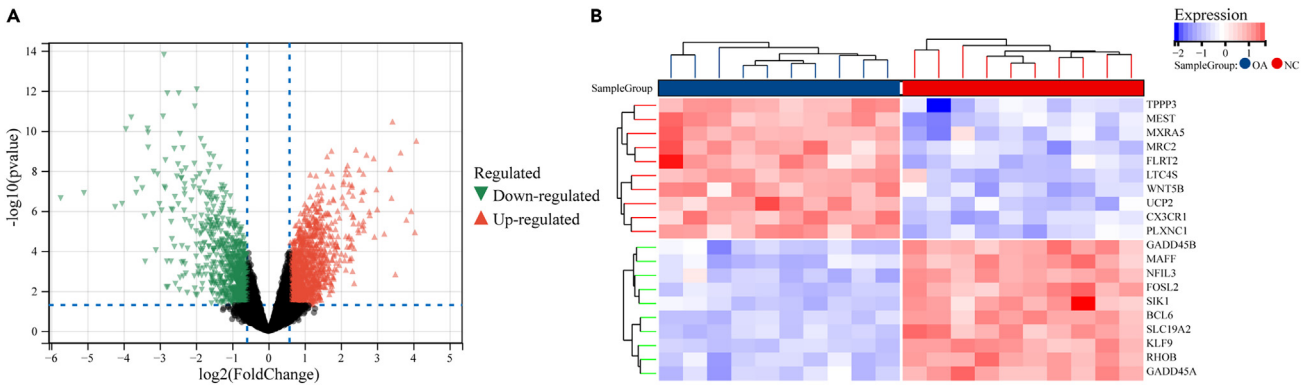

Figure 2. Genes differentially expressed between NC and OA samples

(A) Identification of differentially expressed genes. The volcano plot shows the differentially expressed genes in the GSE55235 dataset, green indicates genes highly expressed in NC, red indicates genes highly expressed in OA, and gray indicates genes with no significant change.

(B) The heatmap displays the top twenty upregulated and downregulated differentially expressed genes in NC or OA samples.

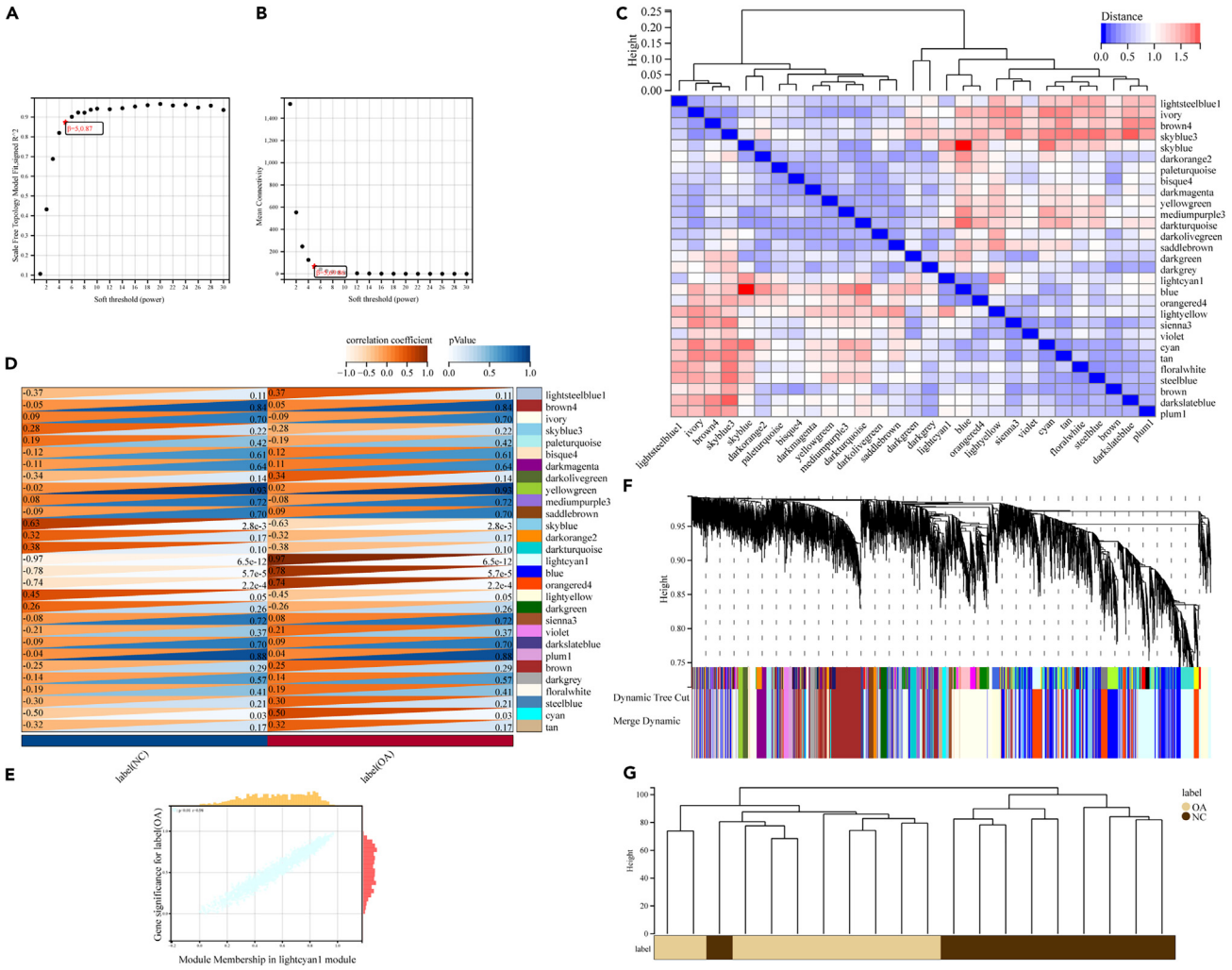

Figure 3. Results of WGCNA

(A) Fit indices of the corresponding scale-free topology models under different soft thresholds.
(B) The corresponding average connectivity under different soft thresholds.
(C) Eigenvector clustering of different modules.
(D) Heatmap of the correlation of different modules with phenotypes.
(E) Correlation of module membership and gene significance in the lightcyan1 module.
(F) Clustering dendrogram of genes.
(G) Clustered dendrograms of different samples.

in OA. Similarly, we evaluated the mRNA expression levels of these six genes in the GSE55457 dataset and obtained partially similar results to those mentioned previously (Figure S1).

Biological processes and pathways of hub gene enrichment

Using enrichment analysis, we were able to understand the potential biological functions of these genes. Gene ontology (GO) analysis included the analysis of BP, CC, and MF. The results showed that these six genes are mainly engaged in autophagy, the process utilizing autophagic mechanism (Figure 6A), neuron projection, mitochondrion (Figure 6B), transcription factor binding, and Tubin binding (Figure 6C). Kyoto Encyclopedia of Genes and Genomes (KEGG) analysis revealed that five out of six genes are involved in autophagy-related biological processes, including mitophagy, autophagy, FoxO, and Apelin signaling pathways (Figure 6D). The gene set enrichment analysis (GSEA) results indicate that these six genes were related to the p53 signaling pathway, NOD-like receptor signaling pathway, lysosome, glycerol lipid metabolism, antigen processing, and presentation (Table 3). GSEA indicated significant associations of these genes with the p53 signaling and NOD-like receptor signaling pathways, with Normalied Enrichment Score (NES) values >1.5, Nominal (NOM) p values <0.05, and false discovery rate (FDR) q values <0.25, suggesting their roles in OA progression (Figure 6E).

Table 1. Identification of co-expression modules

Module name	Number
bisque4	98
blue	870
brown	727
brown4	33
cyan	204
darkgreen	75
darkgrey	68
dark magenta	126
darkolivegreen	60
darkorange2	34
darkslateblue	30
darkturquoise	71
floralwhite	36
ivory	838
lightcyan1	1594
lightsteelblue1	40
lightyellow	178
mediumpurple3	40
orangered4	631
paleturquoise	61
plum1	46
saddlebrown	62
sienna3	55
skyblue	62
skyblue3	50
steelblue	61
tan	147
violet	60
yellowgreen	55

RT-qPCR validation of the hub genes

RT-qPCR experiments were carried out to verify the bioinformatics results. The results showed that the expression of MYC, BNIP3, GABARAPL1, BAG3, MCL1, and PPARGC1A were markedly different in the normal and IL-1β-induced groups, indicating that the bioinformatics data mining results are more reliable. RT-qPCR validation demonstrated significant expression differences for hub genes between normal and OA groups, with p values <0.05 and fold changes >2. The experimental design included triplicate measurements from samples per group, enhancing the validation's reliability (Figure 7A).

Decreased expression of BNIP3 in osteoarthritis

BNIP3 was selected for further analysis for two reasons. As BNIP3 is centrally located in the hub gene network, it regulates other genes; and the HIF-1α-BNIP3 axis is involved in mitochondrial autophagy. It mitigates OA progression.[17] Western blot analysis quantitatively showed a marked decrease in BNIP3 protein levels in OA samples compared to normal, with a significant statistical difference ($p < 0.05$), supporting BNIP3's role in OA pathogenesis (Figure 7B). Immunofluorescence staining and quantitative analysis showed that the protein expression of BNIP3 in chondrocytes was down-regulated in the inflammatory environment of OA, which is consistent with the decreased mRNA expression of BNIP3 in RT-qPCR ($p < 0.05$) (Figure 7C). The differential expression of BNIP3 protein in the normal group and OA group may be attributed to TBHP promoting the enhancement of chondrocyte oxidative stress capacity, leading to increased Reactive oxygen species (ROS) production, more severe mitochondrial damage, and rapid onset of mitochondrial dysfunction and inhibition of BNIP3 expression.

We assessed the severity of OA using the Osteoarthritis Research Society International (OARSI) score and rated cartilage changes using Safranin-O solid green staining in a surgically induced destabilizing the medial meniscus (DMM) mouse model. A sizable amount of cartilage degradation was observed in the DMM group. OA severity, assessed using OARSI scores, showed significant cartilage degradation in the

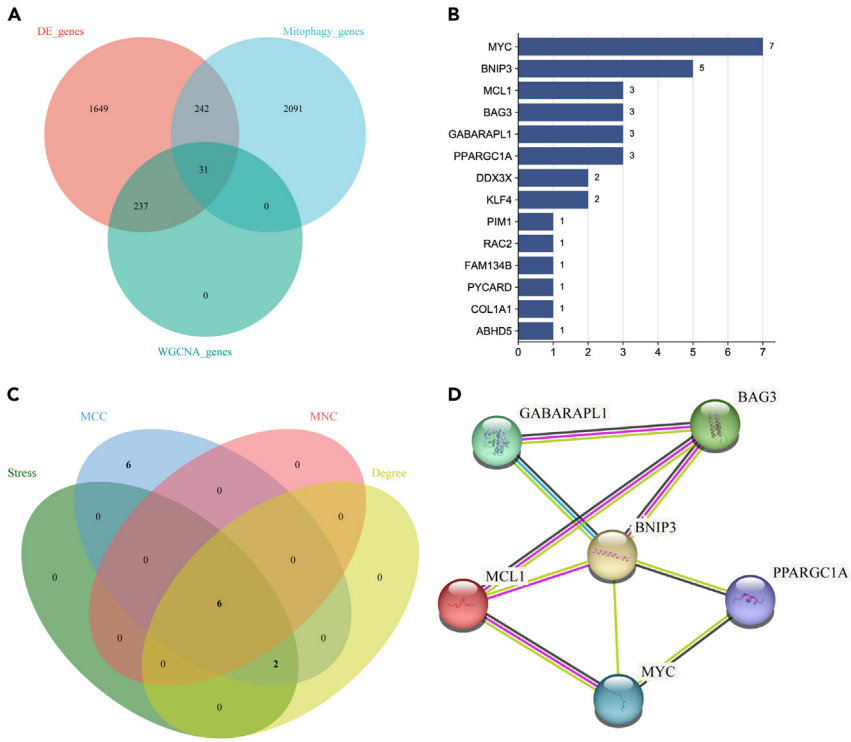

Figure 4. Acquisition and correlation analysis of hub genes

(A) The intersection of 31 hub genes was obtained through the analysis of DEGs, WGCNA of the lightcyan1 module genes, and mitochondrial autophagy-related genes.

(B) Ranking of the connections of 31 central genes. The central genes with lower rankings are hidden, and based on the rankings, the 6 hub genes with the most closely related connections were selected.

(C) The identification of six central genes using four algorithms in CytoHubba and the evaluation of their protein-protein interaction patterns were conducted.

(D) Interaction of 6 hub genes obtained by string database.

DMM group ($p < 0.01$). Safranin-O staining quantitatively corroborated these findings (Figure 7D). In the routine and DMM groups, immunohistochemical staining analysis revealed a decreased ratio of BNIP3-positive cells in the articular cartilage of DMM mice compared to the control group, which was consistent with the results of *in vitro* experiments. These results demonstrate the presence of reduced BNIP3 expression after articular cartilage damage ($p < 0.05$) (Figure 7E).

Developing and validating diagnostic models

A logistic regression algorithm based on GSE55235 was utilized to construct a multi-gene prediction model. The prognostic significance of these genes MYC, BNIP3, GABARAPL1, PPARGC1A, MCL1, and BAG3 in 20 samples was assessed using the cox method (Table 4). The overall prognosis was significantly changed (log-test = 0.0009, sc-test = 0.002, wald-test = 0.493, C-index = 1). The logistic regression model, based on GSE55235, exhibited excellent predictive capability for OA with an Area Under Curve (AUC) value of 0.95. Specific logistic regression parameters were optimized using stepwise regression (Figure 8A). The results showed that our constructed osteoarthritis prediction model had a good predictive effect. Next, we used GSE55457, GSE82107, and GSE169077 as validation datasets for further validation. The results showed that the AUC = 0.99 for the GSE55457 model (Figure 8B) and AUC = 0.94 for the integrated dataset model of GSE82107 and

Table 2. The differential expression results of 6 single genes in the NC and OA groups

Label	Comparison group (mean ± SD)	control group (mean ± SD)	Mann-Whitney test
MYC	NC(10.48 ± 0.59)	OA(7.95 ± 0.57)	1.1e-5
BNIP3	NC(8.06 ± 0.58)	OA(6.45 ± 0.50)	1.1e-5
GABARAPL1	NC(8.93 ± 0.61)	OA(7.57 ± 0.42)	7.6e-5
PPARGC1A	NC(4.07 ± 1.05)	OA(3.86 ± 0.83)	0.58
MCL1	NC(9.79 ± 0.37)	OA(8.51 ± 0.28)	1.1e-5
BAG3	NC(10.11 ± 0.74)	OA(8.20 ± 0.27)	1.1e-5

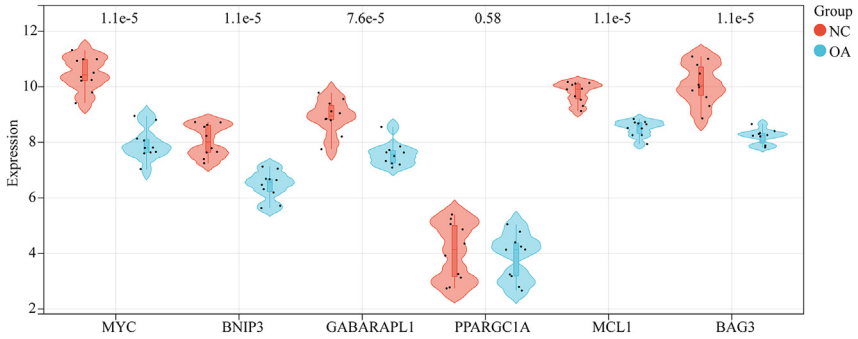

Figure 5. Expression of hub genes in articular cartilage of NC and OA samples in the GSE55235 dataset

GSE169077 (Figure 8C), indicating that the model has some guiding significance for diagnosing OA patients in clinical applications. Validation using GSE55457, GSE82107, and GSE169077 demonstrated consistent predictive performance with AUC values ranging from 0.94 to 0.99, underscoring the model's clinical relevance. Detailed dataset analysis including sample sizes and statistical significance of model performance is provided.

Immune infiltration and immune-related factors

Clinical treatment sensitivity and disease diagnosis are a function of the immunological microenvironment. The CIBERSORT algorithm was used to evaluate the proportion of 22 immune cells in 10 NC samples and 10 OA samples. CIBERSORT analysis indicated significant

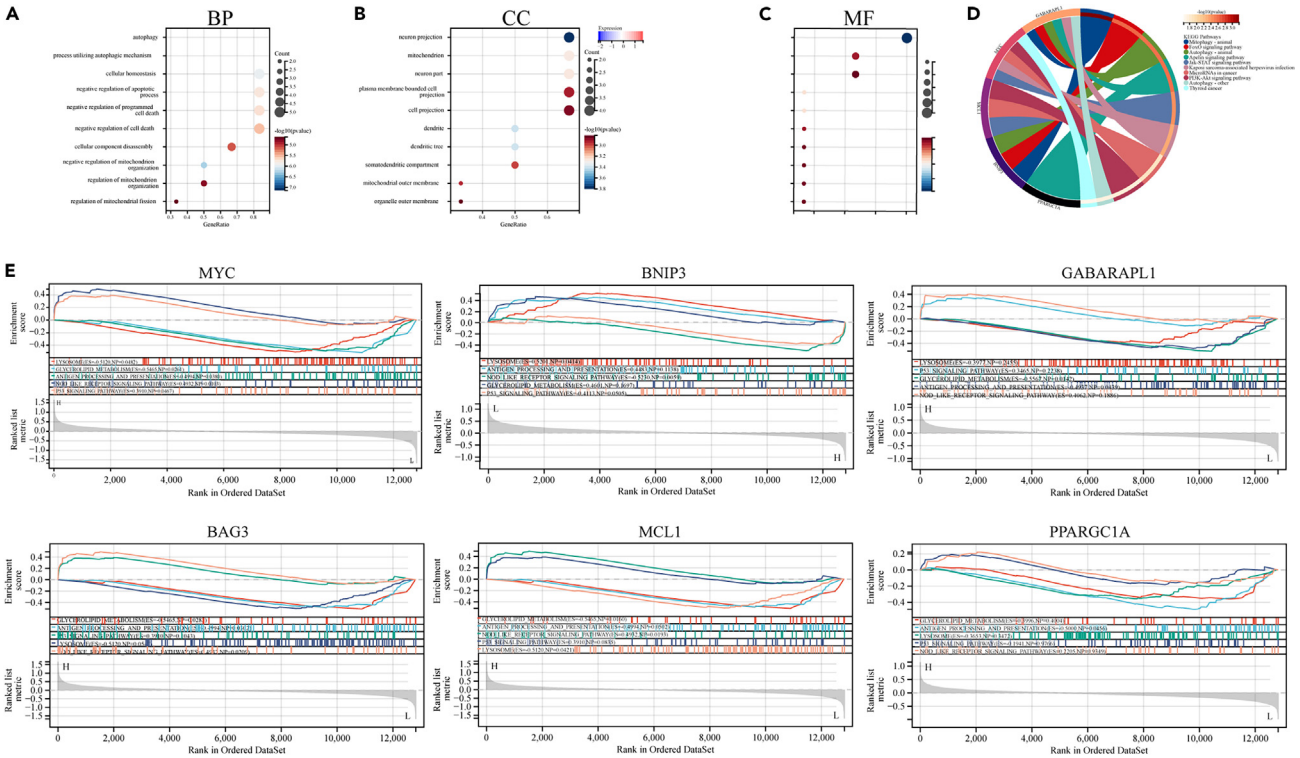

Figure 6. Functional correlation analysis

Hub genes were analyzed by GO, KEGG, and GSEA.

(A) Biological process (BP).

(B) Cellular component (CC).

(C) Molecular function (MF).

(D) KEGG signaling pathway.

(E) GSEA shows the enriched signaling pathways associated with the hub genes that were identified through the filtering. ES, enrichment score; NP, Nominal *p* value, *P < 0.05, **$p < 0.01$.

Table 3. GSEA analysis

Term	ES	NES	*p* value	FDR	FWER
LYSOSOME	−0.5120	1.7271	0.0482	0.5739	0.2610
GLYCEROLIPID_METABOLISM	−0.5465	−1.4643	0.0261	0.6429	0.9020
ANTIGEN_PROCESSING_AND_PRESENTATION	−0.4994	−1.4782	0.0380	0.6595	0.8860
NOD_LIKE_RECEPTOR_SIGNALING_PATHWAY	0.4932	1.5230	0.0103	0.6892	0.8090
P53_SIGNALING_PATHWAY	0.3910	1.3723	0.0467	1.0000	0.9680

differences in immune cell composition between OA and NC samples, providing detailed percentages of each immune cell type and their statistical differences (Figure 9A). Furthermore, we compared immune cell infiltration in the OA and NC samples in the boxplot, as well as the correlation between immune cells (Table 5). The results of immune cell infiltration showed that the percentage of B cells memory, plasma cells, T cells CD4 naive, and mast cells resting in the OA group was significantly higher than that of the NC group; while B cells

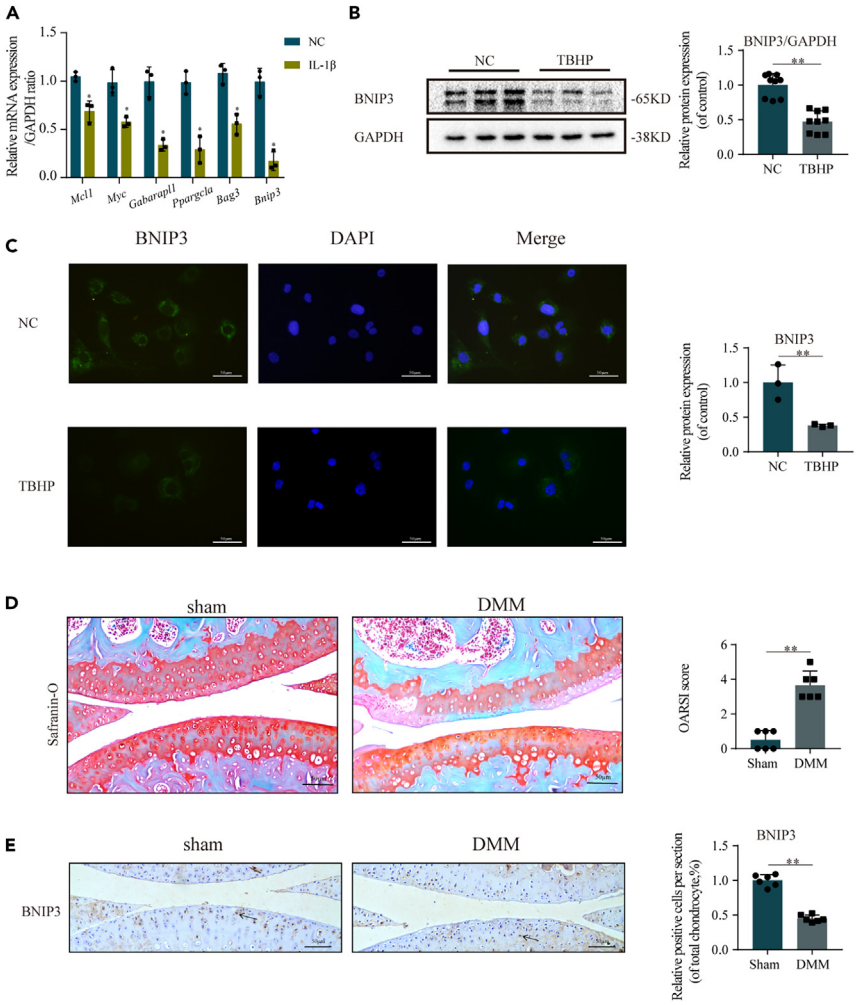

Figure 7. Validation of Hub genes at the cytological and histological levels

(A) RT-PCR results showed mRNA expression levels of Hub genes in mouse chondrocytes in the NC group versus the IL-1β group.

(B) Protein expression of BNIP3 in the NC group versus the TBHP-intervened chondrocyte group.

(C) Immunofluorescence of BNIP3 protein expression in the NC group versus the TBHP-intervened chondrocyte group (bar: 50 μm).

(D) The staining of guanine green and OARSI scores in mouse knee cartilage (bar: 50 μm).

(E) Immunohistochemical staining of BNIP3 in mouse cartilage (bar: 50 μm).

All data represent mean ± SD. *$p < 0.05$, **$p < 0.01$.

Table 4. Muticox analysis

Tag	exp(coef)	Pr(>|z|)	lower 0.95	upper 0.95	coef
MYC	0.791001953782197	0.73215495616388	0.206580043856656	3.02877315352595	0.234454841202
BNIP3	0.841898652166623	0.852474951548842	0.13725446763787	5.16408210762249	−0.1720956375821
GABARAPL1	0.358882992436383	0.378381420922189	0.0367047960585653	3.50899653698081	−1.0247588699804
PPARGC1A	0.945637570779286	0.914300181129945	0.341672547508795	2.61721470393032	−0.0558959009080
MCL1	0.784608184676227	0.87195619850546	0.0410747848987149	14.9875405307402	−0.2425708136064
BAG3	0.223766912891137	0.274510210133301	0.0152605125092237	3.28112383346008	−1.4971503363435

naive, T cells CD4 memory resting, natural killer (NK) cells active, and the percentage of B cells naive, T cells CD4 memory resting, NK cells activated, and mast cells activated were significantly lower than the NC group (Figure 9B). Comparative analysis of immune cell types showed significant correlations among different immune cells in chondrocytes ($p < 0.05$) (Figure 9C). After further exploring the relationship between hub genes and immune infiltration, we conducted a correlation analysis of gene expression levels and immune cell contents of the selected hub genes. The results showed a strong association between hub genes and immune infiltration. Specifically, we found that MYC, BNIP3, GABARAPL1, MCL1, and BAG3 were highly positively correlated with resting CD4 memory T cells and enabled mast cells. Meanwhile, MYC, BNIP3, GABARAPL1, MCL1, and BAG3 were significantly and negatively correlated with plasma cells, B cells memory, and mast cells resting (Figure 9D).

Analysis of drug-gene interactions, related-proteins subcellular localization, and molecular dockings

A protein's subcellular localization identifies its biological function. The protein subcellular localization of MYC, BNIP3, GABARAPL1, PPARGC1A, MCL1, and BAG3 was predicted using public compartments database. The subcellular localization of key proteins was predicted with high confidence scores, indicating their functional relevance in specific cellular compartments (Figure 10A). The development of potential therapeutic agents targeting genes could serve as a specific therapeutic strategy. Using data from DrugBank and Metascape databases,[18] two candidate drugs were identified. Acetylsalicylic acid is a drug that targets MYC, and isosorbide targets MCL1 (Table 6). Acetylsalicylic acid is associated with stimulating autophagy as well as inhibiting apoptosis. Isosorbide is thought to inhibit cellular senescence and maintain normal oxidative stress homeostasis. Autodock Vina calculated the binding energies of the two candidate drugs with two proteins, as well as their binding poses and interactions. The binding energy is defined as the reduction in energy required for the entire system after the protein and molecule are bound. Generally, a binding energy of −4.25 kcal/mol indicates a certain interaction between the receptor protein and the ligand. The receptor (PDB structure of MYC is 6QB6, and the PDB structure of MCL1 is 6E16) was docked with the respective ligands. The protein and ligand files were converted to PDBQT format, water molecules were removed, and polar hydrogen atoms were added. The docking pocket was set to the entire protein, with a grid point spacing of 0.05 nm. The molecular binding sites between MYC, MCL1, and approved small molecule drugs were calculated separately, and the results showed a binding energy of −5.858 kcal/mol for MYC and acetylsalicylic acid (Figure 10B), and a binding energy of −4.445 kcal/mol for MCL1 and mannitol (Figure 10C), indicating a highly stable binding of the corresponding small molecule drugs with the targets.

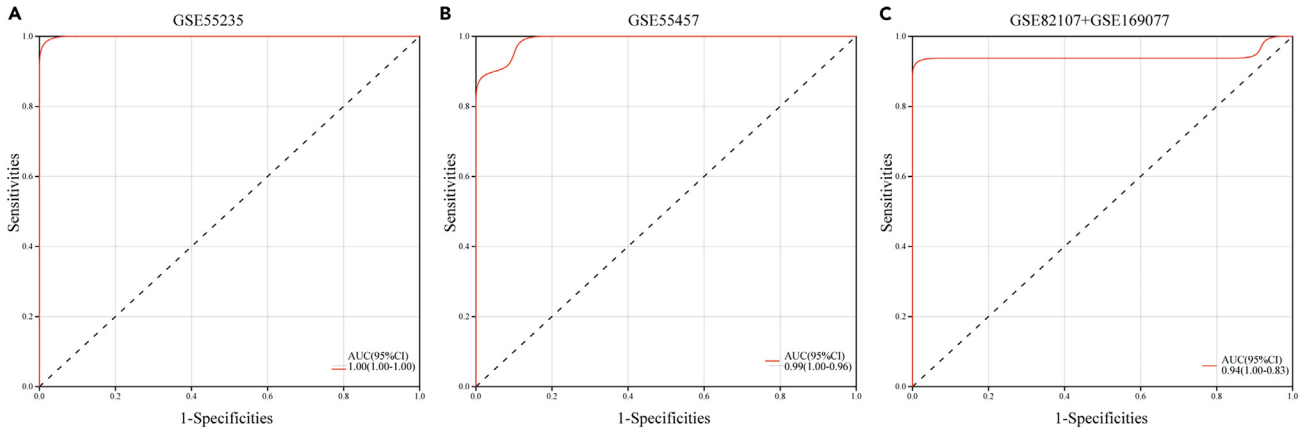

Figure 8. ROC curves and corresponding AUC values for the three diagnostic models

(A) Diagnostic models based on GSE55235.

(B) Diagnostic models based on GSE55457.

(C) Diagnostic models based on integrated datasets of GSE82107 and GSE169077.

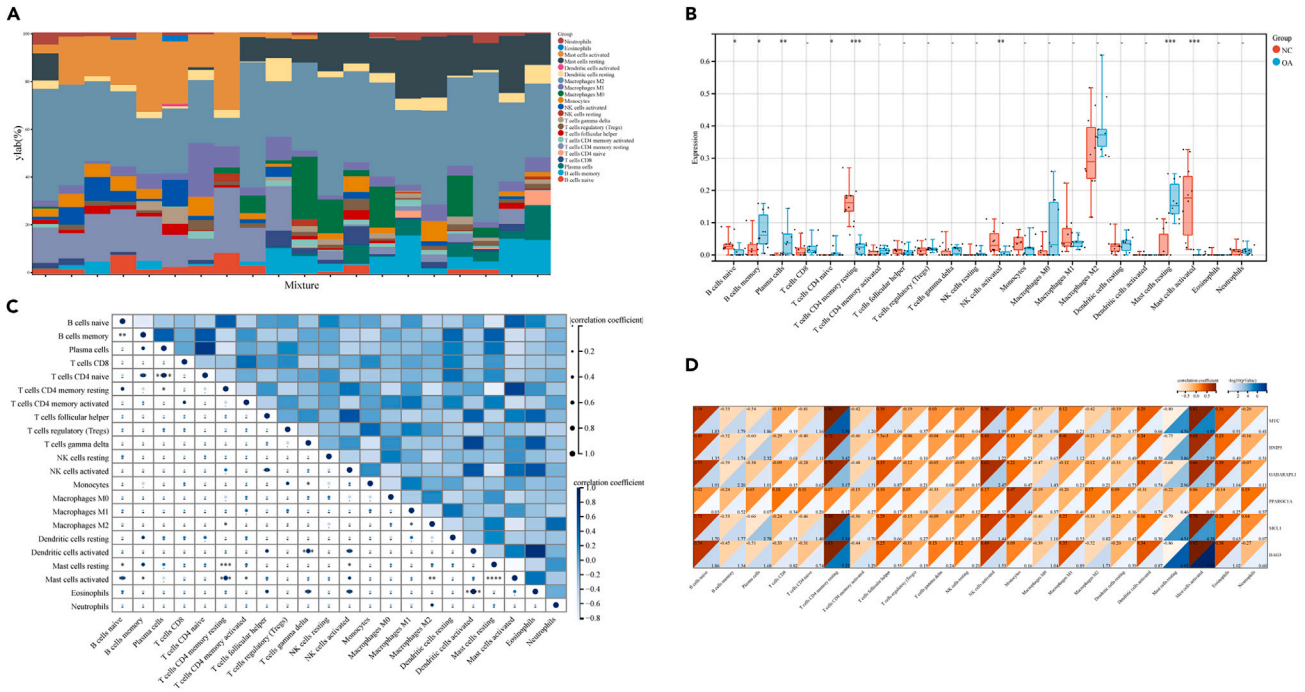

Figure 9. Analysis of immune infiltration

(A) The proportion of 22 immune cells corresponding to each sample in the dataset GSE55235.

(B) The proportion of immune cells in the NC and OA groups.

(C) Correlation of immune cells.

(D) Relationship between hub genes and immune cells.

DISCUSSION

Osteoarthritis is a degenerative disease that results in the breakdown of articular cartilage, thickening of subchondral bone, formation of bone hyperplasia, synovitis, and joint collapse.[19] The pathological process involves increased cartilage catabolism, decreased cartilage anabolism and repair, hypertrophy and death of chondrocytes, impaired autophagy function, osteoclast-mediated bone remodeling, and infiltrating and activating immune cells.[9] Inflammation in OA differs from other autoimmune diseases as it is primarily mediated by the innate immune system. The interaction between the immune system and local tissue damage and metabolic dysfunction further complicates the disease process.[20]

Our study extends these findings by elaborating on the specific molecular pathways involved in OA, such as mitochondrial autophagy and its regulation by key genes. This approach bridges a critical gap in understanding the complex interplay between genetic factors and OA pathogenesis. Despite the expected increase in OA incidence with an aging population, the underlying pathogenesis remains poorly understood, and no disease-modifying drugs are currently available.[21] Our study aimed to investigate the expression pattern and active process of mitochondrial autophagy-related genes in OA using comprehensive and effective bioinformatics methods, to identify new targets for the diagnosis, treatment, and prognosis of early- to mid-stage OA. While the molecular mechanism of mitochondrial autophagy and the immune environment in OA is not fully understood, our study offers new insights that may pave the way for future therapeutic interventions.

Our study aimed to investigate the relationship between mitochondrial autophagy and OA progression. By analyzing RNA expression profiles of OA, we identified 2,159 DEGs and screened 6 genes related to mitochondrial autophagy and OA. Through GO analysis, we found these genes were involved in mitochondrial autophagy, cell homeostasis regulation, and apoptosis. Selective autophagy has been considered an effective approach to eliminating damaged cells under oxidative stress.[22] Previous studies have shown that mitochondrial dysfunction is associated with cartilage matrix breakdown and inhibition of cartilage matrix synthesis, which are correlated with OA.[23] Mitophagy is a fundamental mechanism for maintaining mitochondrial homeostasis and can be used to clear damaged mitochondria, avoid inflammation activation, and inhibit apoptosis.[24] Studies have demonstrated that trehalose promotes the increase of autophagic flux, which can alleviate mitochondrial dysfunction in chondrocytes and relieve the progression of OA. This process is linked with BNIP3-mediated mitotic activity.[25] Moreover, the PPARGC1A gene is essential in regulating mitochondrial biogenesis, while REDD1 controls the mitochondrial biogenesis of articular chondrocytes by regulating PPARGC1A to alleviate OA progression.[26] Studies pointed out that MYC, BNIP3, BAG3, MCL1, PPARGC1A, and GABARAPL1 are commonly involved in regulating mitochondrial function and delaying the progression of degenerative diseases. Abnormal mitochondrial autophagy may be the key link between autophagy function impairment and extracellular matrix (ECM) homeostasis disorder in several degenerative diseases.[27–30] Regarding the clinical applications of our findings, the identified hub genes not only offer a deeper understanding of OA's molecular underpinnings but also serve as promising biomarkers for early detection and therapeutic

Table 5. Immune components results

Label	Comparison group (mean ± SD)	Control group (mean ± SD)	Mann-Whitney test
B cells naive	NC(0.03 ± 0.03)	OA(8.6e-3±0.01)	0.03
B cells memory	NC(0.02 ± 0.03)	OA(0.07 ± 0.06)	0.02
Plasma cells	NC(6.8e-4±1.8e-3)	OA(0.04 ± 0.05)	1.0e-3
T cells CD8	NC(0.01 ± 0.02)	OA(0.02 ± 0.02)	0.28
T cells CD4 naive	NC(0.0e+0 ± 0.0e+0)	OA(9.9e-3±0.02)	0.03
T cells CD4 memory resting	NC(0.16 ± 0.05)	OA(0.02 ± 0.02)	1.8e-4
T cells CD4 memory activated	NC(6.8e-3±0.01)	OA(0.01 ± 0.01)	0.07
T cells follicular helper	NC(0.02 ± 0.01)	OA(0.01 ± 0.01)	0.38
T cells regulatory (Tregs)	NC(0.01 ± 0.01)	OA(0.02 ± 0.01)	0.38
T cells gamma delta	NC(0.01 ± 0.02)	OA(0.01 ± 0.01)	0.23
NK cells resting	NC(3.4e-3±0.01)	OA(4.6e-3±9.4e-3)	0.39
NK cells activated	NC(0.04 ± 0.04)	OA(6.1e-3±9.6e-3)	9.7e-3
Monocytes	NC(0.04 ± 0.03)	OA(0.02 ± 0.03)	0.26
Macrophages M0	NC(0.01 ± 0.02)	OA(0.08 ± 0.10)	0.19
Macrophages M1	NC(0.06 ± 0.06)	OA(0.04 ± 0.02)	0.58
Macrophages M2	NC(0.31 ± 0.12)	OA(0.39 ± 0.10)	0.14
Dendritic cells resting	NC(0.03 ± 0.03)	OA(0.03 ± 0.02)	0.55
Dendritic cells activated	NC(1.1e-3±3.4e-3)	OA(0.0e+0 ± 0.0e+0)	0.37
Mast cells resting	NC(0.03 ± 0.05)	OA(0.17 ± 0.06)	3.7e-4
Mast cells activated	NC(0.17 ± 0.12)	OA(2.0e-3±5.2e-3)	1.1e-4
Eosinophils	NC(3.3e-3±7.6e-3)	OA(0.0e+0 ± 0.0e+0)	0.17
Neutrophils	NC(0.01 ± 0.01)	OA(0.01 ± 0.01)	0.73

targets. The differential expression and pathway involvement of these genes suggest their potential role in diagnostic panels or as candidates for potential drug development aimed at modulating mitochondrial autophagy pathways to halt or reverse OA progression.

In contrast to rheumatoid arthritis (RA), synovial immune activation in OA exhibits distinctive characteristics, aiding in the differentiation between mild RA and inflammatory OA.[31] This distinction is critical for patient stratification, diagnosis, and guiding treatment interventions.[32] Early stages of OA are marked by the infiltration of inflammatory Th1/17 cells, underscoring a complex interplay between immune cells and humoral immunity, which is believed to drive the pathogenesis of autoimmune arthritis and related diseases.[33] The cytokine profile in synovial fluid mirrors the effector and regulatory T cell composition within the synovium,[34] with elevated expression of CCR5, CCR3, and CD161 among $CD4^+$T cells in the joints indicating significant immune activation.[35] Moreover, mast cells within the synovial tissue, known for their role in structural damage through the release of mediators such as tryptase, contribute to inflammation, cartilage degradation, and chondrocyte apoptosis in OA.[36] Our investigation into immune infiltration disparities between normative and OA cohorts reveals significant variances in the prevalence of plasma cells, $CD4^+$T cells, NK cells, and mast T cells in OA patients, aligning with findings from prior studies.[37–39] This analysis illuminates the nuanced immune landscape of OA, offering insights into the disease's immunopathology.

We validated the expression levels of hub genes in normal cartilage and OA models by RT-qPCR, western blot, immunofluorescence, and immunohistochemistry. Significant differences in mRNA expression levels of MYC, BNIP3, MCL1, GABARAPL1, BAG3, and PPARGC1A were observed between the normal and OA groups. Additionally, we address potential confounding factors and alternative explanations for the observed correlations, enhancing the scientific rigor of our study. Finally, we retrieved two drugs targeting the aforementioned genes from DrugBank and Metascape databases. Acetylsalicylic acid (aspirin) can inhibit the activity of cyclooxygenase (COX).[40] Acetylsalicylic acid active metabolite, salicylate, stimulates autophagy flux and slows down aging by inhibiting acetyltransferase EP300,[41] additionally, it reduces chondrocyte apoptosis and cartilage degradation in knee osteoarthritis by inhibiting MMPs, NO, and NF-κB signaling.[42,43] Isosorbide can be used to correct the damaged redox balance between superoxide and nitric oxide, improve calcium circulation and contractility by reducing sarcoplasmic Ca^{2+} leakage, and alleviate vascular sclerosis caused by mitochondrial oxidative stress. It is also used for the treatment of congestive heart failure.[44] Studies have shown that isosorbide can inhibit the senescence of mesenchymal stem cells, reduce senescence-related galactosidase (SA-β-gal) activity, and p21 expression.[45] In addition, we conducted molecular docking experiments to confirm the binding sites of acetylsalicylic acid and nitrobenzene with their respective key proteins MYC and MCL1, with corresponding binding hydrogen bonds TYR-385, ARG-263. The potential drugs showed high binding energy with the key targets, stability, and potential to reduce off-target effects. These findings can serve as valuable resources for further drug development and clinical applications. Our molecular docking results provide detailed insights into the interaction between these drugs and target proteins, confirming their potential therapeutic applications in OA.

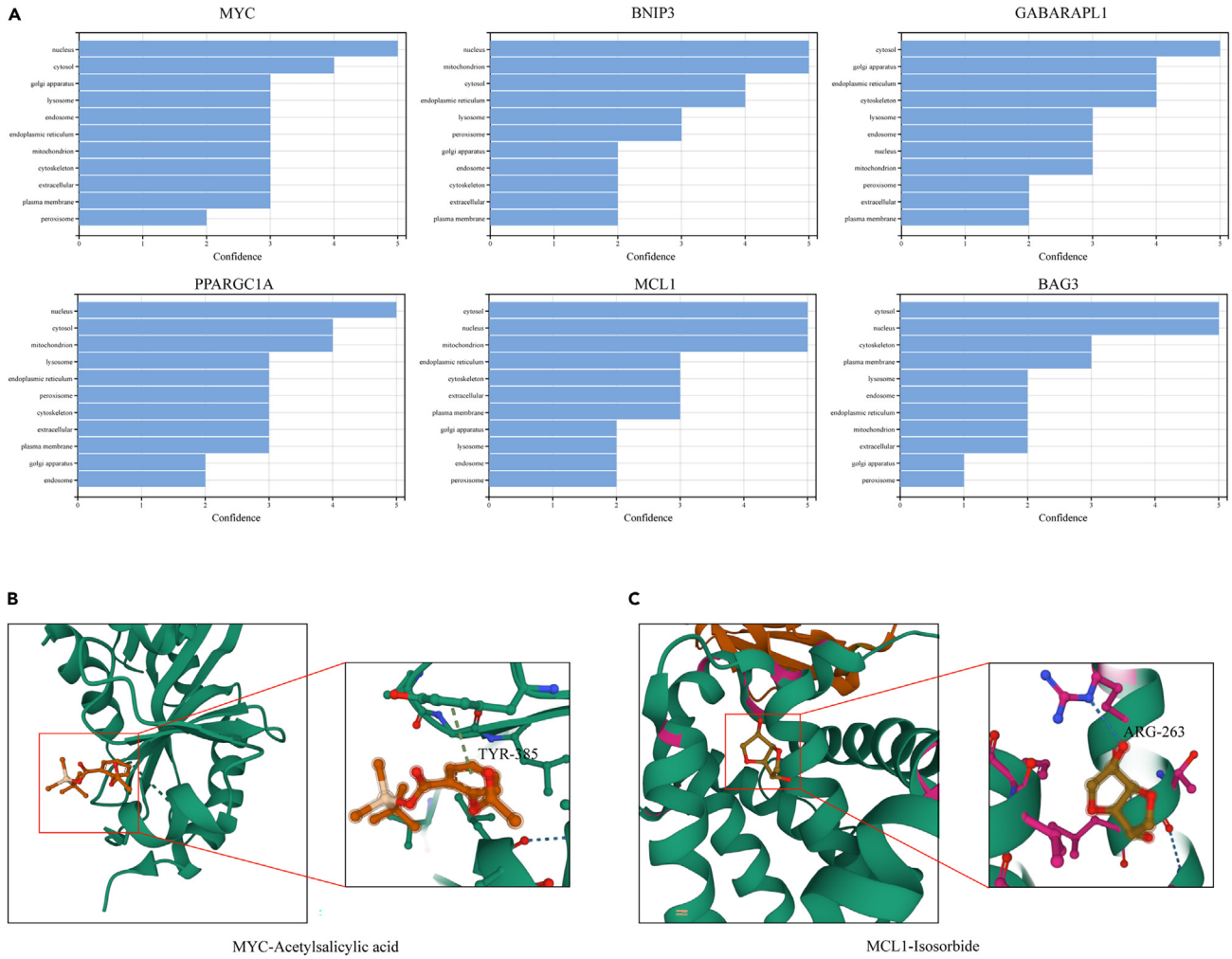

Figure 10. Protein subcellular localization and molecular docking structure of hub genes

(A) Protein subcellular localization of hub genes.

(B) Molecular docking structure of MYC and acetylsalicylic acid, hydrogen bonding of the binding sites is TYR-385.

(C) Molecular docking structure of MCL1 and isosorbide, hydrogen bonding of the binding sites is ARG-263.

A limitation of this study is that gender differences were not fully controlled, which could result in some genes being more significantly expressed in females than males in the gene expression analysis. To mitigate this limitation and enhance the reliability of our findings, future studies will incorporate more rigorous control of gender variables, allowing for a more nuanced understanding of how sex differences may influence gene expression and OA progression.

These results not only highlight the clinical relevance of our findings but also delineate a clear path for future research, particularly in exploring the translational potential of these discoveries into clinical applications. By elucidating the complex molecular mechanisms

Table 6. Molecular docking

Gene Symbol	Gene ID	Description	Subcellular location (Protein Atlas)	Drug (DrugBank)
MYC	4609	MYC proto-oncogene, bHLH transcription factor	Nucleoplasm (enhanced)	Acetylsalicylic acid
BNIP3	664	BCL2 interacting protein 3		
GABARAPL1	23710	GABA type A receptor-associated proteins like 1	Vesicles (approved)	
PPARGC1A	10891	PPARG coactivator 1 alpha	Nucleoplasm (supported)	
MCL1	4170	MCL1 apoptosis regulator, BCL2 family member	Mitochondria (enhanced)	Isosorbide
BAG3	9531	BAG cochaperone 3	Cytosol (supported)	

underlying OA and proposing potential therapeutic targets, our study lays the groundwork for developing innovative treatment strategies. Our results suggest a pronounced association between mitochondrial autophagy and OA progression, revealing the significance of specific hub genes such as MYC, BNIP3, GABARAPL1, MCL1, PPARGC1A, and BAG3. These genes, as evidenced by their differential expression and involvement in key biological processes and pathways, may contribute to the development and exacerbation of OA through their roles in mitochondrial function and cellular stress responses.

Limitations of the study

However, this study also has some limitations. Firstly, the sample study did not exclude the gender factor, which may affect the universality of the results. Secondly, the data mainly came from articular cartilage tissue, lacking validation for surrounding tissues, which may limit the application of the diagnostic model and require further validation through clinical trials to determine the value of the diagnostic model. Finally, further validation of the expression of related genes can be conducted in other animal models.

RESOURCE AVAILABILITY

Lead contact

Further information and requests for resources and reagents should be directed to and will be fulfilled by the lead contact, Professor Fengjing Guo (guofjdoc@163.com).

Materials availability

This study did not generate new unique reagents.

Data and code availability

- This study analyzes existing, publicly available data. The sources for the datasets are listed in the key resources table.
- This study does not report the original code. All codes were used in this study in alignment with recommendations made by authors of R packages in their respective user's guide, which can be accessed at https://www.r-project.org/. All code used in the analyses is deposited on https://www.jianguoyun.com/p/DUTcSZsQjf26Cxjtr_oEIAA.
- Any additional information required to reanalyze the data used in this study is available from the lead contact upon request.
- Publicly available datasets were analyzed in this study. These data can be found Database: GSE55235, GSE55457, GSE82107, GSE169077.

ACKNOWLEDGMENTS

This study was supported by the National Natural Science Foundation of China (82372475 and 82172498). The PCR and western blot experiments were performed at the Experimental Medicine Research Center, Tongji Hospital, Huazhong University of Science and Technology. Dr. Genchun Wang and Dr. Xiong Zhang served as guarantors of this study, ensuring the integrity and accuracy of the data.

AUTHOR CONTRIBUTIONS

G.W. and X.Z. conceived and planned the study, and supervised the analysis work. G.W., X.Z., and J.X. conducted the analysis and drafted the initial manuscript. Z.G. and L.H. critically reviewed the integrity and credibility of the data analysis. K.S. and F.G. revised the manuscript and were responsible for the integrity of data acquisition and statistical analysis. All authors agreed to submit this manuscript, read and approve the final version, and take full responsibility for its content, including the accuracy of the data and the fidelity of the experiment to the registration agreement and its statistical analysis. Each author has unrestricted access to all data.

DECLARATION OF INTERESTS

The authors declare no competing interests.

STAR★METHODS

Detailed methods are provided in the online version of this paper and include the following:

SUPPLEMENTAL INFORMATION

Supplemental information can be found online at https://doi.org/10.1016/j.isci.2024.110741.

Received: November 18, 2023
Revised: February 5, 2024
Accepted: August 12, 2024
Published: August 15, 2024

REFERENCES

1. Park, D.R., Kim, J., Kim, G.M., Lee, H., Kim, M., Hwang, D., Lee, H., Kim, H.S., Kim, W., Park, M.C., et al. (2020). Osteoclast-associated receptor blockade prevents articular cartilage destruction via chondrocyte apoptosis regulation. Nat. Commun. *11*, 4343. https://doi.org/10.1038/s41467-020-18208-y.
2. Story Jovanova, O., Nedeljkovic, I., Spieler, D., Walker, R.M., Liu, C., Luciano, M., Bressler, J., Brody, J., Drake, A.J., Evans, K.L., et al. (2018). DNA Methylation Signatures of Depressive Symptoms in Middle-aged and Elderly Persons: Meta-analysis of Multiethnic Epigenome-wide Studies. JAMA Psychiatr. *75*, 949–959. https://doi.org/10.1001/jamapsychiatry.2018.1725.
3. Huang, J., Zhao, L., Fan, Y., Liao, L., Ma, P.X., Xiao, G., and Chen, D. (2019). The microRNAs miR-204 and miR-211 maintain joint homeostasis and protect against osteoarthritis progression. Nat. Commun. *10*, 2876. https://doi.org/10.1038/s41467-019-10753-5.
4. Ma, Z., Tao, C., Sun, L., Qi, S., Le, Y., Wang, J., Li, C., Liu, X., Zhang, J., and Zhao, J. (2019). In Situ Forming Injectable Hydrogel For Encapsulation Of Nanoiguratimod And Sustained Release Of Therapeutics. Int. J. Nanomed. *14*, 8725–8738. https://doi.org/10.2147/IJN.S214507.
5. Yao, Q., Wu, X., Tao, C., Gong, W., Chen, M., Qu, M., Zhong, Y., He, T., Chen, S., and Xiao, G. (2023). Osteoarthritis: pathogenic signaling pathways and therapeutic targets. Signal Transduct. Targeted Ther. *8*, 56. https://doi.org/10.1038/s41392-023-01330-w.
6. Duong, V., Oo, W.M., Ding, C., Culvenor, A.G., and Hunter, D.J. (2023). Evaluation and Treatment of Knee Pain: A Review. JAMA *330*, 1568–1580. https://doi.org/10.1001/jama.2023.19675.
7. Duan, R., Xie, H., and Liu, Z.Z. (2020). The Role of Autophagy in Osteoarthritis. Front. Cell Dev. Biol. *8*, 608388. https://doi.org/10.3389/fcell.2020.608388.
8. Liu, Z., Wang, T., Sun, X., and Nie, M. (2023). Autophagy and apoptosis: regulatory factors of chondrocyte phenotype transition in osteoarthritis. Hum. Cell *36*, 1326–1335. https://doi.org/10.1007/s13577-023-00926-2.
9. Chen, P., Zheng, L., Wang, Y., Tao, M., Xie, Z., Xia, C., Gu, C., Chen, J., Qiu, P., Mei, S., et al. (2019). Desktop-stereolithography 3D printing of a radially oriented extracellular matrix/mesenchymal stem cell exosome bioink for osteochondral defect regeneration. Theranostics *9*, 2439–2459. https://doi.org/10.7150/thno.31017.
10. Alva, V., Nam, S.Z., Söding, J., and Lupas, A.N. (2016). The MPI bioinformatics Toolkit as an integrative platform for advanced protein sequence and structure analysis. Nucleic Acids Res. *44*, W410–W415. https://doi.org/10.1093/nar/gkw348.
11. Liu, X., Xiao, H., Peng, X., Chai, Y., Wang, S., and Wen, G. (2022). Identification and comprehensive analysis of circRNA-miRNA-mRNA regulatory networks in osteoarthritis. Front. Immunol. *13*, 1050743. https://doi.org/10.3389/fimmu.2022.1050743.
12. Xia, L., and Gong, N. (2022). Identification and verification of ferroptosis-related genes in the synovial tissue of osteoarthritis using bioinformatics analysis. Front. Mol. Biosci. *9*, 992044. https://doi.org/10.3389/fmolb.2022.992044.
13. Liu, H., Deng, Z., Yu, B., Liu, H., Yang, Z., Zeng, A., and Fu, M. (2022). Identification of SLC3A2 as a Potential Therapeutic Target of Osteoarthritis Involved in Ferroptosis by Integrating Bioinformatics, Clinical Factors and Experiments. Cells *11*, 3430. https://doi.org/10.3390/cells11213430.
14. Zhang, Y., Zhu, T., He, F., Chen, A.C., Yang, H., and Zhu, X. (2021). Identification of Key Genes and Pathways in Osteoarthritis via Bioinformatic Tools: An Updated Analysis. Cartilage *13*, 1457S–1464S. https://doi.org/10.1177/19476035211008975.
15. Xu, W., Wang, X., Liu, D., Lin, X., Wang, B., Xi, C., Kong, P., and Yan, J. (2023). Identification and validation of hub genes and potential drugs involved in osteoarthritis through bioinformatics analysis. Front. Genet. *14*, 1117713. https://doi.org/10.3389/fgene.2023.1117713.
16. Zeng, J., Jiang, X., Jiang, M., Cao, Y., and Jiang, Y. (2023). Bioinformatics analysis of hub genes as osteoarthritis prognostic biomarkers. Sci. Rep. *13*, 22894. https://doi.org/10.1038/s41598-023-48446-1.
17. Lin, J., Guo, Z., Zheng, Z., Hou, L., Xu, J., Liu, Q., Du, T., Guo, F., and Jing, X. (2023). Desferoxamine protects against hemophilic arthropathy through the upregulation of HIF-1α-BNIP3 mediated mitophagy. Life Sci. *312*, 121172. https://doi.org/10.1016/j.lfs.2022.121172.
18. Zhou, Y., Zhou, B., Pache, L., Chang, M., Khodabakhshi, A.H., Tanaseichuk, O., Benner, C., and Chanda, S.K. (2019). Metascape provides a biologist-oriented resource for the analysis of systems-level datasets. Nat. Commun. *10*, 1523. https://doi.org/10.1038/s41467-019-09234-6.
19. Hu, S., Zhang, C., Ni, L., Huang, C., Chen, D., Shi, K., Jin, H., Zhang, K., Li, Y., Xie, L., et al. (2020). Stabilization of HIF-1alpha alleviates osteoarthritis via enhancing mitophagy. Cell Death Dis. *11*, 481. https://doi.org/10.1038/s41419-020-2680-0.
20. Zhuo, Q., Yang, W., Chen, J., and Wang, Y. (2012). Metabolic syndrome meets osteoarthritis. Nat. Rev. Rheumatol. *8*, 729–737. https://doi.org/10.1038/nrrheum.2012.135.
21. Varela-Eirin, M., Loureiro, J., Fonseca, E., Corrochano, S., Caeiro, J.R., Collado, M., and Mayan, M.D. (2018). Cartilage regeneration and ageing: Targeting cellular plasticity in osteoarthritis. Ageing Res. Rev. *42*, 56–71. https://doi.org/10.1016/j.arr.2017.12.006.
22. Kraft, C., Peter, M., and Hofmann, K. (2010). Selective autophagy: ubiquitin-mediated recognition and beyond. Nat. Cell Biol. *12*, 836–841. https://doi.org/10.1038/ncb0910-836.
23. Ansari, M.Y., Khan, N.M., Ahmad, I., and Haqqi, T.M. (2018). Parkin clearance of dysfunctional mitochondria regulates ROS levels and increases survival of human chondrocytes. Osteoarthritis Cartilage *26*, 1087–1097. https://doi.org/10.1016/j.joca.2017.07.020.
24. Nakahira, K., Haspel, J.A., Rathinam, V.A.K., Lee, S.J., Dolinay, T., Lam, H.C., Englert, J.A., Rabinovitch, M., Cernadas, M., Kim, H.P., et al. (2011). Autophagy proteins regulate innate immune responses by inhibiting the release of mitochondrial DNA mediated by the NALP3 inflammasome. Nat. Immunol. *12*, 222–230. https://doi.org/10.1038/ni.1980.
25. Tang, Q., Zheng, G., Feng, Z., Chen, Y., Lou, Y., Wang, C., Zhang, X., Zhang, Y., Xu, H., Shang, P., and Liu, H. (2017). Trehalose ameliorates oxidative stress-mediated mitochondrial dysfunction and ER stress via selective autophagy stimulation and autophagic flux restoration in osteoarthritis development. Cell Death Dis. *8*, e3081. https://doi.org/10.1038/cddis.2017.453.
26. Alvarez-Garcia, O., Matsuzaki, T., Olmer, M., Plate, L., Kelly, J.W., and Lotz, M.K. (2017). Regulated in Development and DNA Damage Response 1 Deficiency Impairs Autophagy and Mitochondrial Biogenesis in Articular Cartilage and Increases the Severity of Experimental Osteoarthritis. Arthritis Rheumatol. *69*, 1418–1428. https://doi.org/10.1002/art.40104.
27. Tian, X., Teng, J., and Chen, J. (2021). New insights regarding SNARE proteins in autophagosome-lysosome fusion. Autophagy *17*, 2680–2688. https://doi.org/10.1080/15548627.2020.1823124.
28. Tahrir, F.G., Knezevic, T., Gupta, M.K., Gordon, J., Cheung, J.Y., Feldman, A.M., and Khalili, K. (2017). Evidence for the Role of BAG3 in Mitochondrial Quality Control in Cardiomyocytes. J. Cell. Physiol. *232*, 797–805. https://doi.org/10.1002/jcp.25476.
29. Cen, X., Chen, Y., Xu, X., Wu, R., He, F., Zhao, Q., Sun, Q., Yi, C., Wu, J., Najafov, A., and Xia, H. (2020). Pharmacological targeting of MCL-1 promotes mitophagy and improves disease pathologies in an Alzheimer's disease mouse model. Nat. Commun. *11*, 5731. https://doi.org/10.1038/s41467-020-19547-6.
30. Lin, Q., Li, S., Jiang, N., Jin, H., Shao, X., Zhu, X., Wu, J., Zhang, M., Zhang, Z., Shen, J., et al.

(2021). Inhibiting NLRP3 inflammasome attenuates apoptosis in contrast-induced acute kidney injury through the upregulation of HIF1A and BNIP3-mediated mitophagy. Autophagy *17*, 2975–2990. https://doi.org/10.1080/15548627.2020.1848971.

31. Tu, B., Fang, R., Zhu, Z., Chen, G., Peng, C., and Ning, R. (2023). Comprehensive analysis of arachidonic acid metabolism-related genes in diagnosis and synovial immune in osteoarthritis: based on bulk and single-cell RNA sequencing data. Inflamm. Res. *72*, 955–970. https://doi.org/10.1007/s00011-023-01720-4.
32. Penatti, A., Facciotti, F., De Matteis, R., Larghi, P., Paroni, M., Murgo, A., De Lucia, O., Pagani, M., Pierannunzii, L., Truzzi, M., et al. (2017). Differences in serum and synovial CD4+ T cells and cytokine profiles to stratify patients with inflammatory osteoarthritis and rheumatoid arthritis. Arthritis Res. Ther. *19*, 103. https://doi.org/10.1186/s13075-017-1305-1.
33. Paulissen, S.M.J., van Hamburg, J.P., Dankers, W., and Lubberts, E. (2015). The role and modulation of CCR6+ Th17 cell populations in rheumatoid arthritis. Cytokine *74*, 43–53. https://doi.org/10.1038/nri2094.
34. McInnes, I.B., and Schett, G. (2007). Cytokines in the pathogenesis of rheumatoid arthritis. Nat. Rev. Immunol. *7*, 429–442. https://doi.org/10.3390/biomedicines10092111.
35. Nees, T.A., Zhang, J.A., Platzer, H., Walker, T., Reiner, T., Tripel, E., Moradi, B., and Rosshirt, N. (2022). Infiltration Profile of Regulatory T Cells in Osteoarthritis-Related Pain and Disability. Biomedicines *10*, 2111. https://doi.org/10.3390/biomedicines10092111.
36. Buckley, M.G., Walters, C., Wong, W.M., Cawley, M.I., Ren, S., Schwartz, L.B., and Walls, A.F. (1997). Mast cell activation in arthritis: detection of alpha- and beta-tryptase, histamine and eosinophil cationic protein in synovial fluid. Clin. Sci. *93*, 363–370. https://doi.org/10.1042/cs0930363.
37. Park, Y.B., Kim, J.H., Ha, C.W., and Lee, D.H. (2021). Clinical Efficacy of Platelet-Rich Plasma Injection and Its Association With Growth Factors in the Treatment of Mild to Moderate Knee Osteoarthritis: A Randomized Double-Blind Controlled Clinical Trial As Compared With Hyaluronic Acid. Am. J. Sports Med. *49*, 487–496. https://doi.org/10.1177/0363546520986867.
38. Faust, H.J., Zhang, H., Han, J., Wolf, M.T., Jeon, O.H., Sadtler, K., Peña, A.N., Chung, L., Maestas, D.R., Jr., Tam, A.J., et al. (2020). IL-17 and immunologically induced senescence regulate response to injury in osteoarthritis. J. Clin. Invest. *130*, 5493–5507. https://doi.org/10.1172/JCI134091.
39. Wang, Q., Lepus, C.M., Raghu, H., Reber, L.L., Tsai, M.M., Wong, H.H., von Kaeppler, E., Lingampalli, N., Bloom, M.S., Hu, N., et al. (2019). IgE-mediated mast cell activation promotes inflammation and cartilage destruction in osteoarthritis. Elife *8*, e39905. https://doi.org/10.7554/eLife.39905.
40. Vane, J.R., and Botting, R.M. (2003). The mechanism of action of aspirin. Thromb. Res. *110*, 255–258. https://doi.org/10.1016/s0049-3848(03)00379-7.
41. Pietrocola, F., Castoldi, F., Maiuri, M.C., and Kroemer, G. (2018). Aspirin-another caloric-restriction mimetic. Autophagy *14*, 1162–1163. https://doi.org/10.1080/15548627.2018.1454810.
42. Wluka, A.E., Ding, C., Wang, Y., Jones, G., Urquhart, D.M., and Cicuttini, F.M. (2015). Aspirin is associated with reduced cartilage loss in knee osteoarthritis: Data from a cohort study. Maturitas *81*, 394–397. https://doi.org/10.1016/j.maturitas.2015.04.015.
43. Yoon, J.B., Kim, S.J., Hwang, S.G., Chang, S., Kang, S.S., and Chun, J.S. (2003). Non-steroidal anti-inflammatory drugs inhibit nitric oxide-induced apoptosis and dedifferentiation of articular chondrocytes independent of cyclooxygenase activity. J. Biol. Chem. *278*, 15319–15325. https://doi.org/10.1074/jbc.M212520200.
44. Munzel, T., Gori, T., Keaney, J.F., Jr., Maack, C., and Daiber, A. (2015). Pathophysiological role of oxidative stress in systolic and diastolic heart failure and its therapeutic implications. Eur. Heart J. *36*, 2555–2564. https://doi.org/10.1093/eurheartj/ehv305.
45. Xu, J., Huang, Z., Lin, L., Fu, M., Song, Y., Shen, Y., Ren, D., Gao, Y., Su, Y., Zou, Y., et al. (2015). miRNA-130b is required for the ERK/FOXM1 pathway activation-mediated protective effects of isosorbide dinitrate against mesenchymal stem cell senescence induced by high glucose. Int. J. Mol. Med. *35*, 59–71. https://doi.org/10.3892/ijmm.2014.1985.
46. Chang, J.W., Liu, S.C., Lin, Y.Y., He, X.Y., Wu, Y.S., Su, C.M., Tsai, C.H., Chen, H.T., Fong, Y.C., Hu, S.L., et al. (2023). Nesfatin-1 Stimulates CCL2-dependent Monocyte Migration And M1 Macrophage Polarization: Implications For Rheumatoid Arthritis Therapy. Int. J. Biol. Sci. *19*, 281–293. https://doi.org/10.7150/ijbs.77987.
47. Hu, X., Ni, S., Zhao, K., Qian, J., and Duan, Y. (2022). Bioinformatics-Led Discovery of Osteoarthritis Biomarkers and Inflammatory Infiltrates. Front. Immunol. *13*, 871008. https://doi.org/10.3389/fimmu.2022.871008.
48. Cheng, Q., Chen, X., Wu, H., and Du, Y. (2021). Three hematologic/immune system-specific expressed genes are considered as the potential biomarkers for the diagnosis of early rheumatoid arthritis through bioinformatics analysis. J. Transl. Med. *19*, 18. https://doi.org/10.1186/s12967-020-02689-y.
49. Qin, J., Zhang, J., Wu, J.J., Ru, X., Zhong, Q.L., Zhao, J.M., and Lan, N.H. (2023). Identification of autophagy-related genes in osteoarthritis articular cartilage and their roles in immune infiltration. Front. Immunol. *14*, 1263988. https://doi.org/10.3389/fimmu.2023.1263988.
50. Stelzer, G., Rosen, N., Plaschkes, I., Zimmerman, S., Twik, M., Fishilevich, S., Stein, T.I., Nudel, R., Lieder, I., Mazor, Y., et al. (2016). The GeneCards Suite: From Gene Data Mining to Disease Genome Sequence Analyses. Curr. Protoc. Bioinformatics *54*, 1.30.1–1.30.33. https://doi.org/10.1002/cpbi.5.
51. Meng, J., Du, H., Lv, H., Lu, J., Li, J., and Yao, J. (2022). Identification of the osteoarthritis signature gene PDK1 by machine learning and its regulatory mechanisms on chondrocyte autophagy and apoptosis. Front. Immunol. *13*, 1072526. https://doi.org/10.3389/fimmu.2022.1072526.
52. Liberzon, A., Birger, C., Thorvaldsdóttir, H., Ghandi, M., Mesirov, J.P., and Tamayo, P. (2015). The Molecular Signatures Database (MSigDB) hallmark gene set collection. Cell Syst. *1*, 417–425. https://doi.org/10.1016/j.cels.2015.12.004.
53. Yao, X., Sun, K., Yu, S., Luo, J., Guo, J., Lin, J., Wang, G., Guo, Z., Ye, Y., and Guo, F. (2021). Chondrocyte ferroptosis contribute to the progression of osteoarthritis. J. Orthop. Translat. *27*, 33–43. https://doi.org/10.1016/j.jot.2020.09.006.
54. Yao, X., Jing, X., Guo, J., Sun, K., Deng, Y., Zhang, Y., Guo, F., and Ye, Y. (2019). Icariin Protects Bone Marrow Mesenchymal Stem Cells Against Iron Overload Induced Dysfunction Through Mitochondrial Fusion and Fission, PI3K/AKT/mTOR and MAPK Pathways. Front. Pharmacol. *10*, 163. https://doi.org/10.3389/fphar.2019.00163.
55. Shen, W., Song, Z., Zhong, X., Huang, M., Shen, D., Gao, P., Qian, X., Wang, M., He, X., Wang, T., et al. (2022). Sangerbox: A comprehensive, interaction-friendly clinical bioinformatics analysis platform. iMeta *1*, e36. https://doi.org/10.1002/imt2.36.
56. Coat, J., Demoersman, J., Beuzit, S., Cornec, D., Devauchelle-Pensec, V., Saraux, A., and Pers, J.O. (2015). Anti-B lymphocyte immunotherapy is associated with improvement of periodontal status in subjects with rheumatoid arthritis. J. Clin. Periodontol. *42*, 817–823. https://doi.org/10.1111/jcpe.12433.
57. Lai, D., Tan, L., Zuo, X., Liu, D., Jiao, D., Wan, G., Lu, C., Shen, D., and Gu, X. (2021). Prognostic Ferroptosis-Related lncRNA Signatures Associated With Immunotherapy and Chemotherapy Responses in Patients With Stomach Cancer. Front. Genet. *12*, 798612. https://doi.org/10.3389/fgene.2021.798612.
58. Newman, A.M., Liu, C.L., Green, M.R., Gentles, A.J., Feng, W., Xu, Y., Hoang, C.D., Diehn, M., and Alizadeh, A.A. (2015). Robust enumeration of cell subsets from tissue expression profiles. Nat. Methods *12*, 453–457. https://doi.org/10.1038/nmeth.3337.
59. Binder, J.X., Pletscher-Frankild, S., Tsafou, K., Stolte, C., O'Donoghue, S.I., Schneider, R., and Jensen, L.J. (2014). COMPARTMENTS: unification and visualization of protein subcellular localization evidence. Database *2014*, bau012. https://doi.org/10.1093/database/bau012.
60. Wishart, D.S., Feunang, Y.D., Guo, A.C., Lo, E.J., Marcu, A., Grant, J.R., Sajed, T., Johnson, D., Li, C., Sayeeda, Z., et al. (2018). DrugBank 5.0: a major update to the DrugBank database for 2018. Nucleic Acids Res. *46*, D1074–D1082. https://doi.org/10.1093/nar/gkx1037.
61. Kim, S., Chen, J., Cheng, T., Gindulyte, A., He, J., He, S., Li, Q., Shoemaker, B.A., Thiessen, P.A., Yu, B., et al. (2021). PubChem in 2021: new data content and improved web interfaces. Nucleic Acids Res. *49*. D1388-d1395. https://doi.org/10.1093/nar/gkaa971.
62. Berman, H.M., Westbrook, J., Feng, Z., Gilliland, G., Bhat, T.N., Weissig, H., Shindyalov, I.N., and Bourne, P.E. (2000). The Protein Data Bank. Nucleic Acids Res. *28*, 235–242. https://doi.org/10.1093/nar/28.1.235.

STAR★METHODS

KEY RESOURCES TABLE

REAGENT or RESOURCE	SOURCE	IDENTIFIER
GAPDH	Proteintech Group, USA	60004-1-Ig; RRID: AB_2107436
BNIP3	Cell Signaling Technology, USA	#44060
Interleukin-1β (IL-1β)	R&D systems	#401-ML
Tert-Butyl hydroperoxide solution (TBHP)	Sigma-Aldrich ,St Louis, MO, USA	418064
Trypsin	Biosharp Life Sciences, Hefei, Anhui, China	BL527A
Collagenase II	Biosharp Life Sciences, Hefei, Anhui, China	BS164
4% Paraformaldehyde	Biosharp Life Sciences, Hefei, Anhui, China	BL539A
DMEM/F12 medium	Hyclone, Logan, UT, USA	SH30023.01
Fetal bovine serum Excellent	NEWZERUM LIMITED, Upper Riccarton, Christchurch, New Zealand	E500
total RNA extraction kit	Toyobo, Japan	NPK-101
First Strand cDNA Synthesis kit	Toyobo, Japan	RMD-101T
SYBR Green real-time PCR Master Mix	Toyobo, Japan	QPK-201
RIPA lysis buffer	Boster, Wuhan, Hubei, China	AR0102
Protease inhibitors	Boster, Wuhan, Hubei, China	AR1182
Phosphatase inhibitors	Boster, Wuhan, Hubei, China	AR1183
BCA assay kit	Boster, China,	AR0146
DAPI reagent	Boster, Wuhan, Hubei, China	AR1176
TritonX-100	Biofroxx, Germany	143306
DAB staining	Sigma-Aldrich ,St Louis, MO, USA	D8001-5G
EDTA	EDTA decalcifying solution	E1171
Safranin O Stain Solution	Solarbio Life Sciences, Beijing, China	G1067
Fast Green FCF Stain Solution	Solarbio Life Sciences, Beijing, China	G1661
PVDF membranes	Millipore, USA	IPVH00010
SDS-PAGE gels	BioRad, Hercules, CA, USA	4561036
Experimental models: Organisms/strains		
C57BL/6J mouse	GemPharmatech, Nanjing, China	Strain NO.N000013
Oligonucleotides		
Primer for RT-qPCR, see Material and method	Tsingke Biotech,China	https://www.tsingke.com.cn/
Software and algorithms		
ImageJ Version 1.52i	National Institutes of Health	https://www.nih.gov/
R Software 4.1.1.	The R Project	https://www.r-project.org
Pearson	Corrplot (The R package)	https://cran.r-project.org/web/packages/corrplot/index.html
GraphPad Prism Version 7	GraphPad Software	https://www.graphpad.com/
Adobe Photoshop CC Version 19.0	Adobe	https://www.adobe.com/

EXPERIMENTAL MODEL AND STUDY PARTICIPANT DETAILS

Animal experiments and OA model

The Laboratory Animal Center (Tongji Medical College, Huazhong University of Science and Technology, Wuhan, China) approved all animal experimental procedures. (TJH-202201013). This study utilized twelve 7-week-old male C57BL/6J mice. In the sham-operated group, 6 mice were randomly selected. The sham-operated group underwent sham surgery after receiving an intrapulmonary injection of pentobarbital (35 mg/kg). The OA model was then established by destabilizing the medial meniscus (DMM) in 6 mice. The knee joints were gathered

and fixed in 4% paraformaldehyde for further experiments after the mice were sacrificed 8 weeks later. After being stained histologically and immunohistochemically, knee joints were decalcified with 10% EDTA solution for two weeks and integrated into paraffin. We stained specimens with Safranin-O/fast green after cutting them in the sagittal plane to 5mm thicknesses. OARSI (Osteoarthritis Research Society International) scores were used to measure OA progression. In addition, further sections were deparaffinized, antigen extracted, and incubated with anti-BNIP3 antibody, followed by goat anti-rabbit secondary antibody. DAB staining and hematoxylin counterstaining were made on the sections. Under 200x magnification, images were taken with a fluorescence microscope (Evosflauto. Life Technologies, USA) and the number of BNIP3-positive cells was counted.

METHOD DETAILS

Microarrays Data Source and Differential Expression Analysis

We sourced four datasets (GSE55235,[46] GSE55457,[47] GSE82107,[48] GSE169077,[49]) from the GEO database. Selected datasets comprised RNA expression profiles from OA and normal samples. Differential expression analysis was conducted using the R "limma" package with $|log2FC| > 1.5$ and $p < 0.05$ as cutoff values. Data visualization employed "pheatmap" and "ggplot2" packages for depicting DE genes (Table S4).

Mitochondrial autophagy-related genes and WGCNA

Mitochondrial autophagy-related genes (MRGs) were obtained from the Genecards Database,[50] totaling 2364 genes after removing overlaps. WGCNA, performed using the R "WGCNA" package, analyzed the correlation between gene expression patterns and OA phenotypes.[51] We applied dynamic tree-cutting methods for module detection and correlated these with OA traits using module Eigengenes.

Hub Gene Identification and Validation

The intersection of DE genes, WGCNA, and MRGs was examined using the R "VennDiagram" package to identify OA-related hub genes. Expression differences were visualized using violin plots, and the cytoHubba plugin estimated hub gene networks (Table S5). Statistical analyses, including t-test and Mann-Whitney U test, were employed to validate the findings.

Functional enrichment analysis and GSEA

Functional enrichment, encompassing GO and KEGG analysis, used org.Hs.Eg.Deb (R package) for gene annotations, and KEGG for pathway analysis (Table S6). ClusterProfiler package conducted enrichment analysis with $p < 0.05$ as the significance threshold. GSEA,[52] based on pivotal gene expression, categorized genes by logFC and utilized the "enrichplot" package for result visualization.

Obtaining and culturing mouse chondrocytes

Previously described techniques were utilized to isolate and culture chondrocytes.[53] Cartilage was harvested from five-day-old C57BL/6J mice. The primary chondrocytes were resuspended in DMEM/F12 medium, supplemented with 10% fetal bovine serum (FBS), 1% penicillin, and 1% streptomycin sulfate, and cultured at 37°C in an atmosphere containing 5% CO_2. Experiments were conducted using the second-generation chondrocytes.

Regents

Tert-Butyl hydroperoxide solution (TBHP) was acquired from Sigma-Aldrich (St Louis, MO, USA). BNIP3 antibody (USA, #44060) was acquired from Cell Signaling Technology. Proteintech provides GAPDH antibody (USA, 60004-1-Ig, diluted 1:1000).

RT-qPCR validation of the hub genes

Total RNA extraction with a total RNA extraction kit (Toyobo, Japan). The First Strand cDNA Synthesis kit (Toyobo, Japan) was used to synthesize complementary DNA (cDNA) from total RNA. Next, the cDNA was amplified with SYBR Green real-time PCR Master Mix (Toyobo, Japan) using the following cycling conditions: 30 seconds of polymerase activation at 95°C followed by 40 cycles of 95°C for 5 seconds and 60°C for 30 seconds. Internal control was glyceraldehyde-3-phosphate dehydrogenase (GAPDH). CDNA samples were run in triplicate. The primer sequences are used in the key resources table. Normalization of consequences to housekeeping gene glyceraldehyde-3-phosphate dehydrogenase (GAPDH) expression using the $2^{-\Delta\Delta Ct}$ algorithm.

Analyses of western blot

Chondrocytes were seeded at a density of 5x10^5 cells/well in six-well plates and allowed to adhere for 24 hours before being subjected to different treatments. The control group remained untreated, while in the experimental group, chondrocytes were exposed to 50 μM TBHP for 24 hours. Western blot analysis was conducted as previously described.[54] The cells were washed three times with PBS and lysed using RIPA buffer (Boster, China, AR0102) containing a 1% protease inhibitor cocktail, on ice for 30 minutes. The lysate was centrifuged at 13,000 rpm for 20 minutes to collect the supernatant, and protein concentration was determined using a BCA assay kit (Boster, China, AR0146). A total of 25 μg of protein per sample was subjected to electrophoresis on 12% SDS-PAGE gels and transferred onto PVDF membranes (Millipore,

USA). The membranes were blocked with 5% skim milk for one hour at room temperature and incubated with primary antibody overnight at 4°C, followed by secondary antibody for one hour at room temperature. Protein bands were visualized using the ChemiDocTM XRS+ system (Bio-Rad Laboratories, CA, United States) with a chemiluminescent substrate kit (Boster, China), and band density was quantified using ImageJ version 1.48.

Immunofluorescence

A 12-well plate was seeded with chondrocytes. After treatment, the cells were as shown in 4% paraformaldehyde for 15 minutes at room temperature. Following permeabilization with 0.5% TritonX-100 for 20 minutes, the cells were blocked with 5% BSA for 1 hour at room temperature. BNIP3 antibody was then incubated overnight with chondrocytes at 4°C. Cells were treated with goat anti-rabbit secondary antibody for 1 hour in the dark the following day. We incubated the cells with DAPI for 5 minutes after washing them three times with PBS. An Evosflauto fluorescence microscope (Life Technologies, USA) was utilized to obtain the images.

Logistic regression model

Logistic regression is a generalized linear regression analysis model that allows the automatic diagnosis of diseases.[55] OA samples were divided into the response variable 1 in this study, while NC samples were represented by the response variable 0. In the first step, we use stepwise regression analysis to eliminate factors that are insignificant for the response variable and thus streamline the model. The Akaike Information Criterion (AIC) is minimized by iteratively adding or removing variables from the model.[56,57] These significant factors were then fitted to the response variables for logistic regression. Utilize the receiver operating characteristic curve (ROC) and the area under the ROC curve to evaluate the diagnostic efficacy of the constructed model. "stats" and "pROC" packages were used to perform these analyses.

Immune infiltration and immune-related factors analysis

We employed the CIBERSORT system[58] to evaluate immune cell infiltration in the OA microenvironment. This advanced tool, built on linear support vector regression principles, accurately distinguishes among 22 immune cell types, including B cells, T cells, and myeloid cells, by analyzing their specific biomarkers. Our study used gene expression data from the GSE55235 dataset to quantify these cells' relative proportions. We then employed GraphPad Prism to explore the correlation between variations in these immune cells and the identified hub gene, providing insights into immune involvement in OA.

Analysis of protein subcellular localization

The compartment database predicted the subcellular localization of target proteins. Drug-gene interactions were explored using the Drugbank Database and Cytoscape for visualization, while molecular docking involved PubChem and PDB databases for structural analysis.

The compartment database predicted the subcellular localization of target proteins. An overview of the protein's uniform localization can be achieved with a schematic cell.[59]

Analysis of drug-gene interactions and molecular docking

Drug-gene interactions were explored using the Drugbank Database and Cytoscape for visualization. Drugbank Database[60] is used to determine existing and potentially relevant compounds to investigate drug-gene interactions. DrugBank is a repository of chemoinformatics and bioinformatics information on drugs and their targets. Cytoscape was used for data visualization, and molecular structures of ligands and putative proteins were obtained from PubChem,[61] and PDB databases.[62] Molecular docking involved PubChem and PDB databases for structural analysis. Docking simulations were performed by auto dock vina to generate docking structures, and PyMOL2 software was used for visualization.

QUANTIFICATION AND STATISTICAL ANALYSIS

We utilized R Software 4.1.1. Pearson correlation analysis was applied to establish relationships between genes. Group comparisons were conducted using the Chi-square test or Fishe R exact test for categorical variables. Continuous variables were analyzed using the independent Student's t-test for normally distributed data, and the Mann-Whitney U test for non-normally distributed datasets. All tests were two-tailed with a significance level set at $P < 0.05$, ensuring the reliability of our findings. The comprehensive statistical analysis was augmented by GraphPad Prism 7, allowing for a nuanced interpretation of the data. All data represent mean $\pm$ S.D. *$P < 0.05$, **$P < 0.01$.